Image Deblurring for Less Intrusive Iris Capture

Xinyu Huang [†] [‡] Liu Ren[†] Ruigang Yang[‡]

Robert Bosch Research and Technology Center[†]
Palo Alto, CA 94304
{xinyu.huang,liu.ren}@us.bosch.com

University of Kentucky[‡]
Lexington, KY 40507
{xhuan4,ryang}@cs.uky.edu

Abstract

For most iris capturing scenarios, captured iris images could easily blur when the user is out of the depth of field (DOF) of the camera, or when he or she is moving. The common solution is to let the user try the capturing process again as the quality of these blurred iris images is not good enough for recognition. In this paper, we propose a novel iris deblurring algorithm that can be used to improve the robustness and nonintrusiveness for iris capture. Unlike other iris deblurring algorithms, the key feature of our algorithm is that we use the domain knowledge inherent in iris images and iris capture settings to improve the performance, which could be in the form of iris image statistics, characteristics of pupils or highlights, or even depth information from the iris capturing system itself. Our experiments on both synthetic and real data demonstrate that our deblurring algorithm can significantly restore blurred iris patterns and therefore improve the robustness of iris capture.

1. Introduction

It is well known that iris is one of the most accurate biometric modalities to recognize an individual [1]. Algorithms for iris recognition have been well studied and commercialized during the past ten years. However, it is still challenging to make iris biometric systems less intrusive. Most commercial iris biometric systems require users stand very close to the camera ($3 \sim 50$ cm), remain still for several seconds, or even move back and forth according to the voice prompts. This is mainly because human iris is very small and high quality iris images with sufficient resolution (i.e., the minimum diameter of an iris should be larger than 150 pixels [1]) are difficult to capture, especially over a long distance. A desired iris capturing system should have a larger depth of field (DOF), a longer stand-off distance, and a faster capturing speed. In practice, due to the limitations of hardware, most existing iris capturing systems do not meet all of these requirements. As a result, less-than-ideal iris images can be easily produced by these systems, which usually result in recognition failures. The user then needs to use the system multiple times until an ideal iris image is captured, which significantly increases the nonintrusiveness of the whole system. Among all these less-than-ideal iris images, blurred images are often seen. They are generated by these iris capturing systems when the user is out of the depth of field (DOF) of the camera, or when he or she is moving. If blurred iris patterns can be restored for successful recognitions based on image deblurring techniques, the robustness of the iris capturing system can be greatly improved.

Although image deblurring has been widely studied recently [2, 6, 9], most of them do not address the application domain for iris capture and recognition or they do not make good use of characteristics of iris images for iris biometric applications [5]. We believe domain knowledge inherent in iris images and iris capture systems could be used to improve the performance for iris deblurring. Therefore, we propose a novel iris deblurring algorithm that makes use of the prior knowledge obtained from the statistics of iris images, the characteristics of pupil and highlight regions, and the depth information from the capture system. In particular, we introduce a novel method for blur kernel estimation based on depth information, which allows our algorithm to handle iris defocus blur introduced by the delay of the capturing system when the user is moving. We have built an iris capture system that consists of a commercial off-the-shelf (COTS) camera and a depth sensor to evaluate the performance of our algorithm. Our experiments show that our iris deblurring algorithm can significantly restore blurred iris patterns and make iris capture less intrusive.

2. Related Works

Image deblurring is essentially an ill-posed problem. As a result, priors play a very important role to recover a

[1]This work was done while the first author was a visiting student at Robert Bosch Research and Technology Center in Palo Alto, CA.

blurred image. Kang and Park proposed a non-blind deconvolution algorithm to restore clear iris images and further extend the DOF [5]. They estimated the point spread function (PSF) from the focus score that was measured from the high frequency components of the iris regions after eyelashes and eyelids were removed. However, there are two limitations in [5]. First, the working range of the deblurring algorithm is quite limited, only from 1.8 to 6.6 cm away from the camera. As a result, the proposed method is not suitable for a nonintrusive long range iris capturing system in which the illumination might not be perfect and the user needs to move faster. Second, the Gaussian smoothness term used in the algorithm is not the best prior for iris image deblurring because it tends to over-smooth the restored image. Our intuition is that strong priors, especially those computed from iris images themselves can boost the deblurring performance significantly.

Image deblurring could also benefit less intrusive iris capture systems as many of them have been proposed to extend the operational range for iris capture in recent years [7, 3, 13, 4]. For example, Matey and colleagues proposed the Iris on the Move (IOM) system that consisted of multiple synchronized high-speed, high-resolution, and narrow-field-of-view (NFOV) video cameras, in which focus was fixed at a portal around 3 meters away from the camera [7]. This is the first system that could be used in practice for iris capture over long distances with a high throughput (20 persons/min). However, the DOF for each user is still quite limited ($5 \sim 12$ cm). With the limited DOF, it is possible that the same user still needs to pass the portal multiple times until a clear iris image is captured. A high performance iris deblurring algorithm will be desirable for these systems. Wavefront Coding technology (WFC) was applied by Narayanswamy and Silveira on fixed focus cameras to extend the DOF [8]. Smith and colleagues evaluated the performance of WFC based on a series of simulations [10]. They reported that the DOF was increased from 8.2 to 13.5 cm, which was still quite limited. Some other systems [3, 13, 4] could adjust the focus position of lens in operation so that the DOF of these systems could be easily extended to more than 1.5 meters. Even though cameras with high shutter speed were often used in these systems, users still needed to remain still for several seconds so that high quality iris images could be captured. This is because defocus blur can easily happen when the iris of a moving subject is captured in these settings where significant system delay is often seen. The delay is often caused by the slow movements of the pan-tilt unit and the long autofocus time. On the other hand, the depth information (distance from the user to the camera) is usually provided by these systems. Our analysis shows that the depth information could be used for iris deblurring which can enhance the performance of these less intrusive systems. We have built an iris capture system that combines a commercial off-the-shelf (COTS) camera and a depth sensor to evaluate the performance of our deblurring algorithm for iris capture. We use the accurate depth information obtained from the depth sensor to estimate the blur kernel and handle the potential defocus blur introduced by the system delay.

3. Iris Image Deblurring

Iris image deblurring could greatly increase system robustness for iris capture as blurred images are very likely captured by most less intrusive iris capturing systems due to hardware limitations. In many of these systems, there is almost no motion blur where high shutter speed ($\leq 1/320$ seconds) is chosen. As a result, the blur is mainly defocus blur. When video cameras with fixed focus are used, the system delay is usually small. However, as the DOF is quite small, the user could easily move out of the focus range. When cameras with adjustable focus are used, the DOF can be enlarged significantly. However, there is a system delay between the time when the capture event is sent out and the time when the shutter is released for the capture. The delay could consist of several parts including the time to drive the pan-tilt unit, the time to drive the lens to the desired position, and the time to release the shutter and capture the image. Therefore, if a user is moving, there is a difference between the estimated focused depth of the camera and the real depth of the eyes when the iris image is taken. When the depth difference is larger than the DOF of the camera, the defocus blur also occurs.

We discuss our image deblurring solution to the defocus blur problem in this section. We first give a brief introduction to image deblurring techniques in Section 3.1. We then introduce our blur kernel estimation method based on the depth information of the iris capture systems in Section 3.2. Finally, we present how the prior information can be computed from iris images for image deblurring in Section 3.3.

3.1. Background

Image blur can be modeled as a convolution process.

$$I = L \otimes h + n \tag{1}$$

where I, L, h, and n represent the blurred image, unblurred image, point spread function (PSF), and additive noise respectively. For defocus blur, the PSF h depends on the circle of confusion R (Figure 1). For cameras with adjustable focus, R is a function of two parameters: the distance from the object to the lens d and the distance between lens and image plane s [11],

$$R = \frac{Ds}{2}\left|\frac{1}{f} - \frac{1}{d} - \frac{1}{s}\right| \tag{2}$$

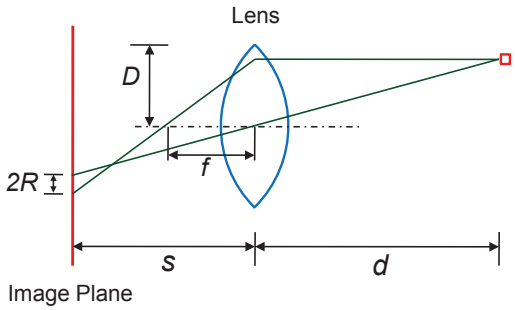

Figure 1. The camera model for computing the circle of confusion R.

where D is the radius of the lens, and f is the focal length of the lens. For cameras with fixed focus s, R is only determined by d. Figure 1 shows the typical camera model to compute R.

The PSF h for the defocus blur is usually modeled as a Gaussian kernel,

$$h = \frac{1}{2\pi\sigma_h^2} e^{-\frac{x^2+y^2}{2\sigma_h^2}}. \quad (3)$$

Because the captured eye region is usually parallel to the image plane, the PSF h is considered as shift-invariant.

Image deblurring relies on image deconvolution to restore the unblurred image L from the blurred image I. The procedure is often formulated in a Bayesian framework [6, 9],

$$P(L|\sigma_h, I) \propto P(I|L, \sigma_h)P(L), \quad (4)$$

where $P(I|L, \sigma_h)$ is the likelihood and $P(L)$ represents the priors on the unblurred image. Assuming the image noise is spatially i.i.d., we can define the likelihood as

$$P(I|L, \sigma_h) \propto \prod_i N(n_i|0, \sigma_n), \quad (5)$$

where $n = I - L \otimes h$ is the image noise.

There are two key issues in this image deconvolution procedure. One is the estimation of the blur kernel, which is characterized by the kernel parameter σ_h. The other one is how to define priors. If the blur kernel is a known input when Equation 4 is solved, this procedure is called non-blind deconvolution or blind deconvolution if otherwise.

3.2. Depth Aware Blur Kernel Estimation

In this section, we discuss the blur kernel estimation assuming the depth information is measured. When a camera with fixed focus are used, it is relatively simple to estimate the kernel. Kang and Park [5] presented an analysis for this situation although the depth information was not used in their system in practice. Our kernel estimation method deals with a more general case, i.e., cameras with adjustable focus. We first compute the focus position based on the measured depth information and then capture the iris image using the estimated focus position. As we mentioned before, there is a depth difference, which is mainly caused by the system delay when a subject is moving. As a result, the estimated focus position is not always desirable, which introduces the defocus blur. The following analysis shows that if we measure the depth difference, we can estimate the kernel parameter σ_h.

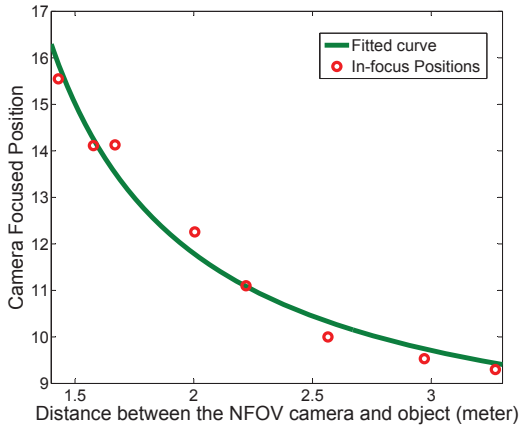

Figure 2. The fitting result for the in-focus positions and the depths based on our proposed model in Equation 6.

As the focus position of the lens p_f is proportional to the distance between the lens and the image plane s, when the circle of confusion R is small enough (i.e., the captured image is in-focus), we can derive the relationship between in-focus position of lens p_f and d based on Equation 2,

$$p_f = \frac{d}{k_1 d + k_2}. \quad (6)$$

After focus positions of in-focus images are measured at different depths, k_1 and k_2 can be easily estimated by curve fitting using Equation 6. Figure 2 shows that there is a strong correlation between the in-focus positions and depth values and such a relationship can be correctly modeled by Equation 6.

As σ_h is proportional to R and s is proportional to p_f, when d is fixed, we can further derive the relationship between σ_h and p_f based on Equation 2,

$$\sigma_h = |k_3 p_f + k_4|. \quad (7)$$

Because we cannot measure σ_h directly, we use the following simple algorithm to estimate σ_h and then compute k_3 and k_4 accordingly:

- Capture in-focus and defocused checkerboard images under different depths and different focus positions.

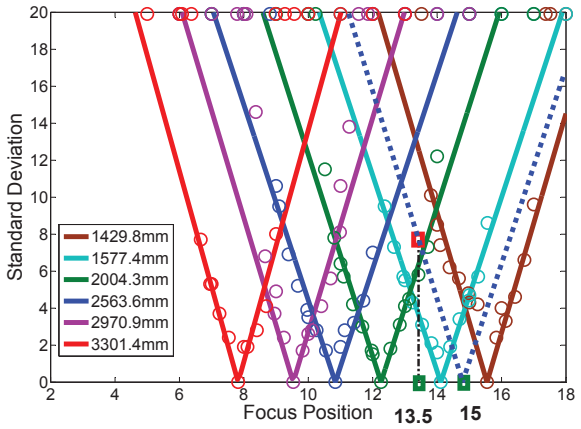

Figure 3. The fitting results for focus positions and the standard deviation σ_h based on the proposed model in Equation 7. The data points on the top are the images severely blurred. It is not feasible to recover these blurred images in practice even with a large kernel size. As a result, they are treated as outliers in the estimation. The dashed blue line is the interpolation between its nearest neighbors. The green square at 15 is the correct in-focus position. The green square at 13.5 is the estimated in-focus position. The red square illustrates the estimated standard deviation σ_h for iris deblurring.

- As in-focus and defocused images are known and only σ_h is unknown, σ_h is estimated by $\arg\min_{\sigma_h} \|I - L \otimes h\|_2^2$.

- k_3 and k_4 are estimated by $\arg\min_{k_3,k_4} \|k_3 p_f + k_4 - \sigma_h\|_2^2$.

Figure 3 shows the fitting results for p_f and σ_h based on Equation 7. Figure 2 and Figure 3 show that it is suitable to use the models described in Equation 6 and Equation 7 for real camera systems even though our derivation is based on a simple thin lens model.

A practical use of Figure 3 is to estimate the blur kernel when the subject is moving. When a user enters the field of view of the capturing system, the 3D positions of eyes are predicted considering the system delay. When the predicted position satisfies the triggering condition for iris capture, the predicted in-focus position $\tilde{p}_f$ is computed using Equation 6 and the image is taken using this focus position. When the correct depth is measured after the system delay, the correct in-focus position $\bar{p}_f$ is also computed. For example, as illustrated in Figure 3, assuming correct in-focus position $\bar{p}_f$ is 15, we can interpolate a new model using precomputed models at position 14 and 16. The new model is illustrated in dashed lines in Figure 3. Assuming the predicted in-focus position $\tilde{p}_f$ is 13.5, we can compute the standard deviation σ_h using Equation 7 and then the image deconvolution becomes a non-blind deconvolution.

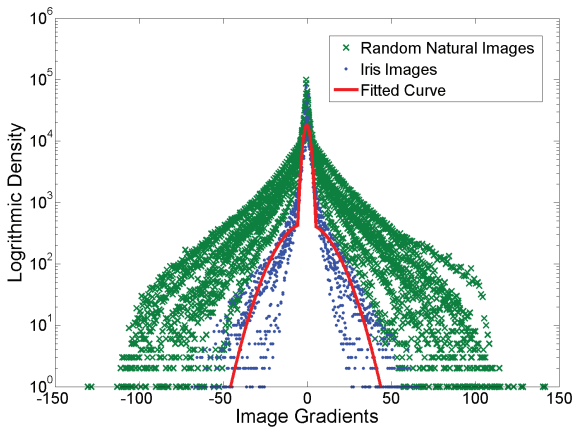

Figure 4. Comparison between the gradient distribution of six iris images and that of six natural images selected randomly. The red curve represents the first prior $P_g(L)$ in our deblurring algorithm.

3.3. Iris Priors

The complete prior term $P(L)$ in Equation 4 consists of three components. The first prior $P_g(L)$ is computed from the distribution of the iris image gradients. The second prior $P_p(L)$ is based on the characteristics of the dark pupil region. And the third prior $P_s(L)$ is computed from the saturated highlight region inside the pupil.

$$P(L) = P_g(L)P_p(L)P_s(L) \tag{8}$$

The first prior makes use of iris image statistics. It has been shown that the natural image gradients have a heavy-tailed distribution [12]. For natural images, the deblurring performance using this prior is much better than the one using Gaussian smoothness prior [6]. For general image deblurring, the distribution could be approximated by a mixture of Gaussian distributions [2], an exponential function such as $|z|^{0.8}$ [6], or a piecewise continuous function [9]. Figure 4 compares the logarithmic gradient distributions computed from both natural and iris images. Six images are randomly selected from each category. The comparison shows that the distribution of general natural images has a larger uncertainty compared with that of iris images. As a result, the distribution of the iris image gradients should be a stronger prior for iris deblurring. In our algorithm, we use two piecewise quadratic functions to approximate the distribution $P_g(L)$ so that the computation is more efficient.

$$P_g(L) \propto \begin{cases} \prod_i e^{a_1(\partial L_i)^2 + b_1}, |\partial L_i| \leq k \\ \prod_i e^{a_2(\partial L_i)^2 + b_2}, |\partial L_i| > k \end{cases} \tag{9}$$

where ∂L_i is the gradient for a pixel and k is a threshold that separates low and high frequency regions of an iris image.

The other two priors ($P_p(L)$ and $P_s(L)$) are computed from the pupil region. We are interested in priors computed

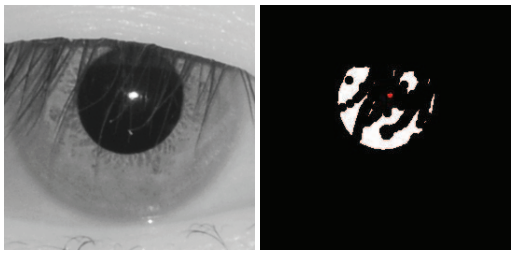

Figure 5. Left: an iris image captured by our system. Right: the masks for the detected pupil region (white) and highlight region (red).

from the pupil region because the dark pupil region is likely to be smooth compared with the nearby iris patterns, and the highlight in the region is likely saturated. Therefore, these two priors are particularly useful to recover nearby iris patterns. We define these two priors based on two observations. First, smooth pupil regions are not sensitive to the defocus blur because these regions tend to have small gradients. Second, saturated highlight region tends to contain the highest intensity. $P_p(L)$ and $P_s(L)$ can be defined as,

$$\begin{aligned} P_p(L) &\propto \prod_{i\in\Omega_1} N(\partial L_i - \partial I_i|0,\sigma_p) \\ P_s(L) &\propto \prod_{i\in\Omega_2} N(L_i - 255|0,\sigma_s), \end{aligned} \tag{10}$$

where Ω_1 is the dark pupil region and Ω_2 is the saturated highlight region within the pupil. Ω_1 and Ω_2 can be detected by standard image processing techniques, such as thresholding, erosion and dilation. Figure 5 shows one typical segmentation result for the pupil region using image thresholding and erosion.

Putting all of these priors together, we can solve the iris deblurring problem using Equation 4, which is equivalent to minimizing the following energy function,

$$\begin{aligned} E \propto & \|I - L \otimes h\|^2 \\ & + \lambda_1(\|a_1(\partial L)^2 + b_1\| \cdot M_1 + \|a_2(\partial L)^2 + b_2\| \cdot M_2) \\ & + \lambda_2(\|\partial L - \partial I\|^2 \cdot M_3 + \|L - 255\|^2 \cdot M_4), \end{aligned} \tag{11}$$

where M_1, M_2, M_3, and M_4 are masks of the low-frequency region, the high-frequency region, the dark pupil region, and the highlight region of the pupil respectively.

We could extend our algorithm from the non-blind deconvolution to a blind deconvolution as estimated PSF h could contain noise propagated from the uncertainty of the measured depth. Assuming the noise of the measured depth has a Gaussian distribution, we can add a Gaussian prior for σ_h and make the algorithm a blind deconvolution. On the other hand, it is computationally expensive and the deblurring performance may not be improved significantly.

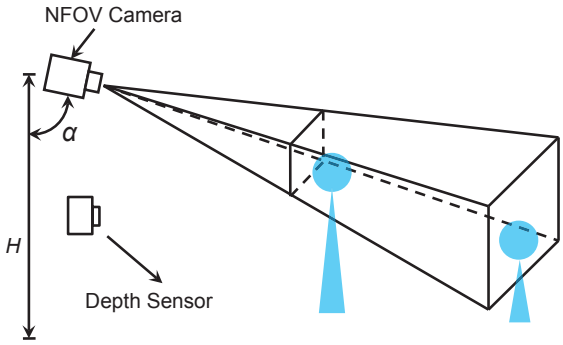

Figure 6. The configuration of the iris capturing system.

4. Experiments

In order to evaluate the performance of our iris deblurring algorithm, we have built a long range iris capuring system to acquire both in-focus and blurred iris images in real scenarios (Section 4.1). We first compare the performance between our deblurring algorithm and the algorithm using the Gaussian prior [5] on synthetic defocused images in Section 4.2. We then evaluate the performance of our algorithm on real blurred iris images in Section 4.3.

4.1. Experimental System Setup

Our iris capture system consists of one NFOV NIR camera with adjustable focus (Canon EOS 40D with a 200 mm lens, 3888×2592 image resolution), one NIR flash, and one depth sensor (SwissRanger SR3000) (see Figure 6). The mounting height H and tilt angle α of the NFOV camera are easily computed such that the standoff distance is from 1.5 meters to 3.5 meters and the captured iris diameter is above 150 pixels. The system delay is between 100 ms and 200 ms, which includes the time to drive the lens and perform the capture. The system could be extended to handle more general scenarios with a pan-tilt unit.

The 3D information measured by the depth sensor plays an important role in our system pipeline (Figure 7). First, face detection and tracking are performed on the intensity image captured by the depth sensor. The eye positions are then estimated based on the upper portion of the detected face. The system also predicts the next 3D eye location for the moving subject using the Kalman filter. Second, the 3D position is used to determine if eyes are within the field of view and correct depth range so that the captured iris images have enough resolutions for successful recognitions. When these two conditions are satisfied, a capture event is sent to the NFOV camera for the iris capture. Third, the depth information is used to control focus position of the NFOV camera dynamically. Finally, the depth information is used to estimate the blur kernel as described in Section 3.2.

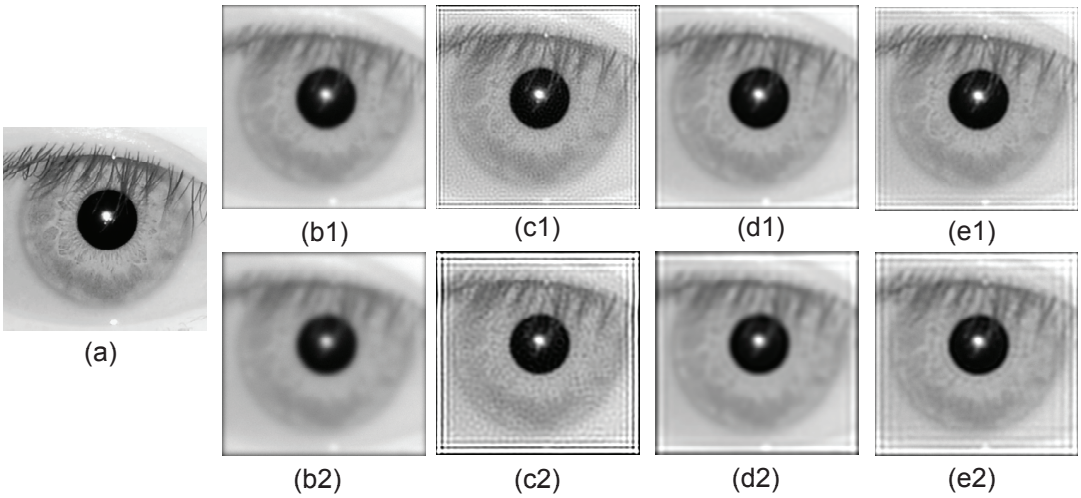

Figure 8. Comparison of iris deblurring algorithms using synthetic data set. (a) Ground truth. (b1) is a blurred image with kernel size 11×11 and $\sigma_h = 2.5$. (b2) is a blurred image with kernel size 25×25 and $\sigma_h = 4$. (c1), (c2), (d1), and (d2) are the results using algorithm [5] with $\lambda = 0.001$ and $\lambda = 0.3$, respectively. The λ is the weight of the Gaussian prior. (e1) and (e2) are the results generated from our algorithm with $\lambda_1 = 0.002$ and $\lambda_2 = 0.5$.

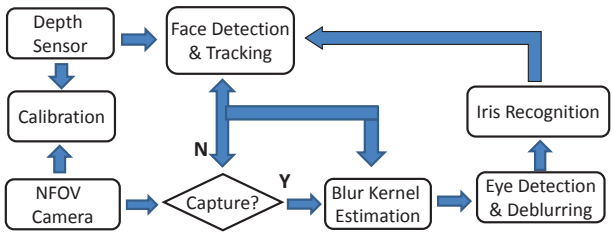

Figure 7. The system pipeline.

4.2. Synthetic Data

We generate the synthetic defocused images by applying known Gaussian kernels to blur the in-focus iris images captured by our system. A small amount of Gaussian noise is also added to these blurred images. Figure 8 shows that our algorithm recovers more iris features than the algorithm using the Gaussian prior [5]. We find that if Gaussian prior is used, the reconstructed images are noisy when λ (i.e., the weight of the Gaussian prior) is small. However, when λ increases, the images are over-smoothed and converge to the blurred input images.

Table 1 shows the root mean square (RMS) errors computed based on the recovered and original images in Figure 8. Our algorithm provides smaller reconstruction errors, especially for more blurred images. We also test the algorithm using Gaussian priors with λ from 0.001 to 0.3. We find that the RMS error decreases as λ increases.

4.3. Real Data

We first use the blurred iris images captured by our system to evaluate the accuracy for the blur kernel estimation.

	(c1), (c2)	(d1), (d2)	(e1), (e2)
RMS	37.50, 51.01	20.43, 28.85	20.41, 27.24

Table 1. The RMS errors based on the original and recovered images using our algorithm and the algorithm in [5]

In Figure 9, the predicted depth is 2.15 m where the correct depth is 2.47 m. The predicted in-focus position is 11.29 and the correct in-focus position is 10.51 based on the calculation using Equation 6. Based on Equation 7, the standard deviation σ_h is 4.1. Figure 9 shows that iris deblurring with standard deviation 4.1 provides us quite clear iris patterns. One the other hand, the deblurring performance degrades if other values are used.

The in-focus and defocused iris images are collected from 28 subjects. Multiple defocused images for each subject are captured around ± 25 cm away from the in-focus position. Each subject is enrolled into the iris database with his or her in-focus iris image. Figure 10 shows the deblurring results for iris images captured with different defocus levels. Note that the size of pupil also changes slightly in Figure 10. This is because the NIR flash and other in-door light sources could cause the iris to dilate when the iris is captured at different depths. When the defocus blur is small, there is no big difference on performance between our algorithm and the algorithm using Gaussian prior [5]. However, the ringing artifacts are obvious from the algorithm as σ_h increases [5]. The last column in Figure 10 shows an example that both algorithms fail to recover. Part of reasons could be that the kernel size is not big enough and the image contains discretization error. However, by using the priors from the pupil region, the ringing effects are reduced significantly.

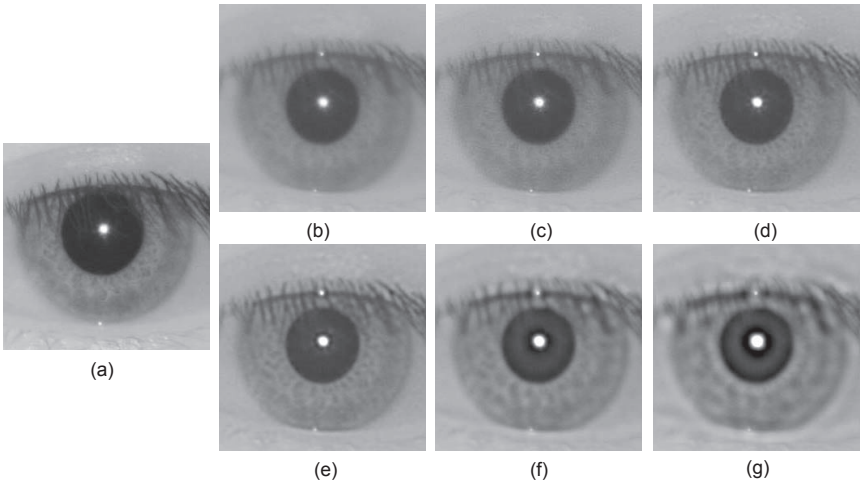

Figure 9. Evaluation of our blur kernel estimation algorithm. (a) An enrolled clear image. (b) The blurred image captured at predicted depth 2.15 m. The predicted in-focus position is 11.29. (c) The iris deblurring result using $\sigma_h = 1.3$. (d) $\sigma_h = 2.7$. (e) $\sigma_h = 4.1$, this value is computed using Equation 6 and Equation 7 with the correct depth at 2.47 m and in-focus position at 10.51. (f) $\sigma_h = 5.5$. (g) $\sigma_h = 7.9$.

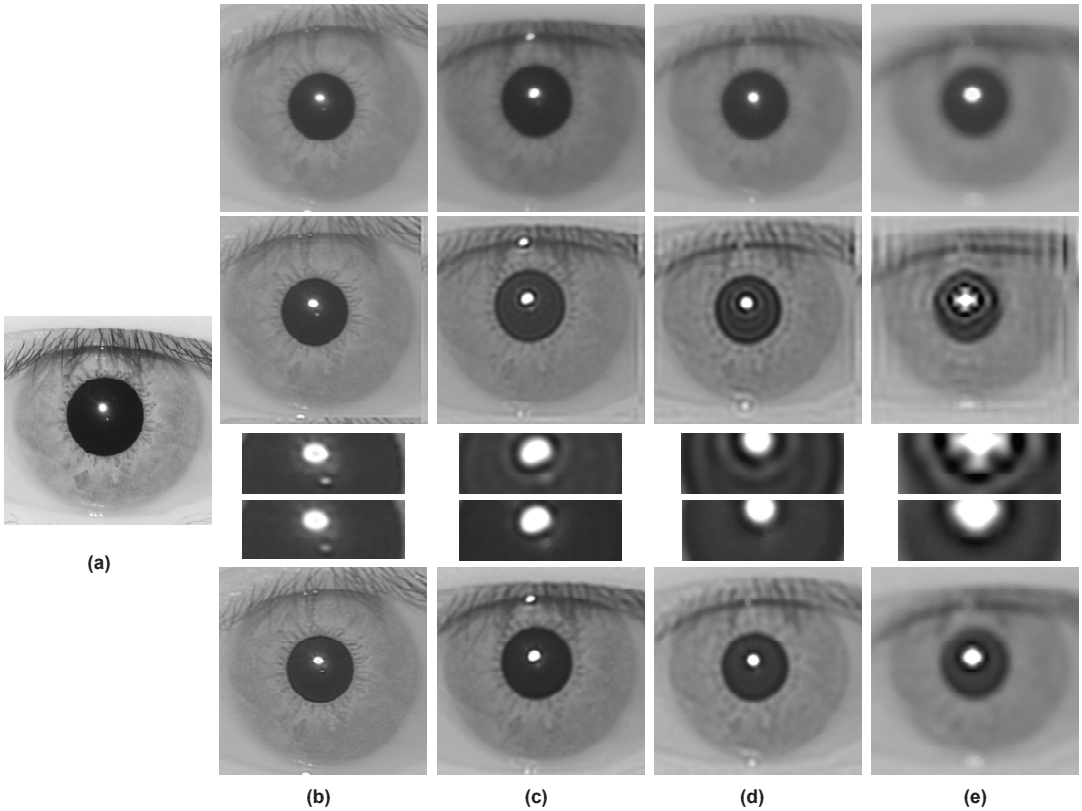

Figure 10. Comparison of iris deblurring algorithms with kernel window size 25×25. (a) In-focus iris image. (b) $\sigma_h = 2.11$. (c) $\sigma_h = 4.3$. (d) $\sigma_h = 5.8$, (e) $\sigma_h = 14.8$. The 1st row shows the captured defocused iris images. The 2nd row shows the deblurring results based on the Gaussian priors. The 3rd row shows the enlarged pupil regions for the iris images on the 2nd row. The 4th row displays the enlarged pupil regions for the iris images on the 5th row. The 5th row shows the corresponding iris deblurring results based on our algorithm.

Figure 11 shows the distribution of the Hamming distance computed between defocused/deblurred images and enrollment images. The defocused images have different defocus levels including seriously blurred images shown in

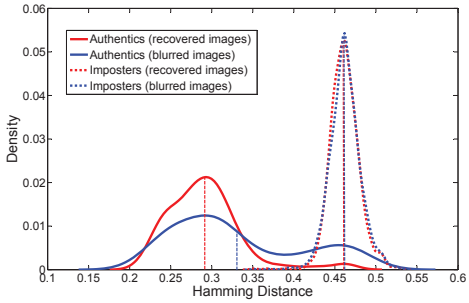

Figure 11. Hamming distance distribution. For the authentic distribution based on recovered images, $\mu = 0.2916$, $\sigma = 0.0458$. For the authentic distribution based on blurred images, $\mu = 0.3311$, $\sigma = 0.0791$. For the imposter distribution based on recovered images, $\mu = 0.4617$, $\sigma = 0.0176$. For the imposter distribution based on blurred images, $\mu = 0.4624$, $\sigma = 0.0187$.

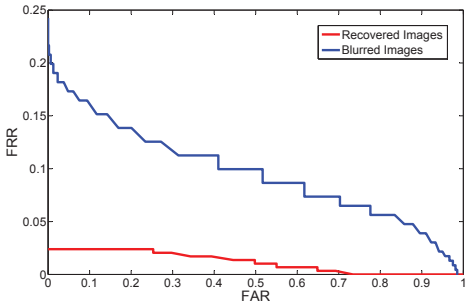

Figure 12. ROC curve comparison. The red ROC curve is computed from enrolled clear images and deblurred images using our algorithm. The blue curve is computed based on the enrolled clear images and blurred images.

Figure 10 (e). When the Hamming distance is less than 0.25, there are no much improvements using our algorithm as the images are already clear enough for recognition. When the Hamming distance is larger than 0.25, our algorithm starts to take effects. The mean of the authentic distribution based on deblurred iris images is reduced by 12% using our algorithm, while this is only reduced by 0.7% using the algorithm with the Gaussian prior [5]. The receiver operation curves (ROC) in Figure 12 show that the recognition errors are significantly reduced by our algorithm.

5. Conclusion

In summary, we have proposed a novel iris deblurring algorithm for less intrusive iris capture. One key feature of our algorithm is that the blur kernel can be accurately estimated using the 3D depth information, which could be provided by many less intrusive iris capture systems. Furthermore, combined with the priors computed from the iris image statistics and characteristics of local regions (pupil area and highlight), our iris deblurring algorithm achieves better performance on both synthetic and real data set compared with the state-of-the-art iris deblurring algorithm. In the future, we will continue to optimize the performance of our deblurring algorithm and collect more data sets for the evaluation.

Acknowledgement

We would like to thank our reviewers for their valuable feedbacks. This work is supported in part by research grants from Robert Bosch LLC, the University of Kentucky Research Foundation, the US Department of Homeland Security, the US National Science Foundation (HCC-0448185 and CPA-0811647).

References

[1] J. Daugman. How iris recognition works. *IEEE Transactions on Circuits and Systems for Video Technology*, 14:21–30, 2004. 1

[2] R. Fergusa, B. Singh, A. Hertzmann, S. T. Roweis, and W. T. Freeman. Removing camera shake from a single photograph. *ACM Transactions on Graphics*, 25:787–794, 2006. 1, 4

[3] G. Guo, M. Jones, and P. Beardsley. A system for automatic iris capturing. Technical report, MERL-TR2005-044, June 2005. 2

[4] X. Huang, J. Gao, and R. Yang. Calibrating pan-tilt cameras with telephoto lenses. In *ACCV*, pages 127–137, 2007. 2

[5] B. J. Kang and K. R. Park. Real-time image restoration for iris recognition systems. *IEEE Transactions on Systems, Man, and Cybernetics, Part B*, 37:1555–1566, Dec. 2007. 1, 2, 3, 5, 6, 8

[6] A. Levin, R. Fergus, F. Durand, and W. T. Freeman. Image and depth from a conventional camera with a coded aperture. *ACM Transactions on Graphics*, 26(70):1–9, 2007. 1, 3, 4

[7] J. Matey, O. Naroditsky, K. Hanna, R. Kolczynski, D. LoIacono, S. Mangru, M. Tinker, T. Zappia, and W. Zhao. Iris on the move: Acquisition of images for iris recognition in less constrained environments. *Proceedings of the IEEE*, 94:1936–1947, 2006. 2

[8] R. Narayanswamy and P. E. X. Silveira. Iris recognition at a distance with expanded imaging volume. In *SPIE 6202: Biometric Technology for Human Identification III*, 2006. 2

[9] Q. Shan, J. Jia, and A. Agarwala. High-quality motion deblurring from a single image. In *SIGGRAPH*, volume 27, 2008. 1, 3, 4

[10] K. N. Smith, V. P. Pauca, A. Ross, T. Torgersen, and M. C. King. Extended evaluation of simulated wavefront coding technology in iris recognition. In *BTAS*, pages 1–7, 2007. 2

[11] G. Surya and M. Subbarao. Depth from defocus by changing camera aperture: A spatial domain approach. In *CVPR*, pages 61–67, 1993. 2

[12] Y. Weiss and W. Freeman. What makes a good model of natural images? In *CVPR*, pages 1–8, 2007. 4

[13] S. Yoon, H. G. Jung, J. K. Suhr, and J. Kim. Non-intrusive iris image capturing system using light stripe projection and pan-tilt-zoom camera. In *Biometrics Workshop, CVPR*, pages 1–7, 2007. 2